Research Article | Vol. 9, No. 11 / 1 November 2019 / Optical Materials Express 4178

Optical Materials EXPRESS

Mechanically robust antireflective moth-eye structures with a tailored coating of dielectric materials

YOUNG JIN YOO,[1,5] YEONG JAE KIM,[1,5] SO-YOUNG KIM,[2] JONG HEON LEE,[1] KYUJUNG KIM,[4] JOO HWAN KO,[1] JI WON LEE,[3] BYOUNG HUN LEE,[2] AND YOUNG MIN SONG[1,*]

[1] *School of Electrical Engineering and Computer Science (EECS), Gwangju Institute of Science and Technology (GIST), 123, Chemdangwagi-ro, Buk-gu, Gwangju 61005, South Korea*
[2] *School of Materials Science and Engineering, Gwangju Institute of Science and Technology, 123 Cheomdangwagi-ro, Buk-gu, Gwangju 61005, South Korea*
[3] *Interior System Plastic Materials Development Team, Hyundai Motor Group, South Korea*
[4] *Department of Cogno-Mechatronics Engineering, Pusan National University, Busan 46241, South Korea*
[5] *These authors contributed equally to this work and should be considered co-first authors*
[*] *ymsong@gist.ac.kr*

Abstract: Bioinspired moth-eye surface provides broadband antireflection features, which significantly enhance performances in optical components/devices. However, their practical uses are strictly limited due to poor mechanical stability of nano-patterns. In this study, we artificially engineered moth-eye structures on polycarbonate substrate through a thin-film coating of mechanically stable dielectric materials (i.e., Al_2O_3, Cr_2O_3, ZrO_2, and TiO_2 etc). The geometry of Al_2O_3-coated moth-eye surface is designed by considering the effective medium theory and confirmed by calculation of diffraction efficiency based on a rigorous coupled-wave analysis method. The tailored Al_2O_3-coating on moth eye surface exhibit the improved hardness while maintaining high optical transmittance.

1. Introduction

Suppression of light reflection at an optical interface between two materials of different refractive indices is a crucial issue in many optical components/devices including transparent windows, imaging lens, polymer optics, solar cells, and light-emitting diodes (LEDs). The performance of optical components or devices is fairly limited by the Fresnel reflection loss at the top surface of optical medium. Traditionally, thin film technology is commonly used for mass production of antireflective coatings, however, there are still some drawbacks such as limited antireflection (AR) ranges, thermal mismatch, and material selection problems [1–10]. Beyond multilayered structures, over the past few decades, the biomimetic subwavelength structures (SWSs), originally inspired by corneal of night active insects (e.g., moth-eye), have been well developed with various nanofabrication methods including laser interference lithography, nanoimprint, metal thermal dewetting process, focused ion beam (FIB) milling, and self-assembly nanosphere lithography [11–25]. These AR SWSs with broadband and omnidirectional reflection features have also been applied to various research fields such as, optical imaging, transparent windows, displays, LEDs, photovoltaic and photocatalytic devices [13–15,26–41].

Despite of the advantage of AR SWSs, transferring this technology from bench-top status to successful industrial level is limited due to poor mechanical stability of moth-eye nano-patterns. For instance, in practical applications such as display, windows, and eye-glasses, the AR SWSs are exposed to external physical contacts (e.g., scratches and/or pressures), which influences the AR performance. This undesired effect is particularly noticeable in the situation of using polymeric

#372481 https://doi.org/10.1364/OME.9.004178
Journal © 2019 Received 12 Jul 2019; revised 19 Sep 2019; accepted 19 Sep 2019; published 2 Oct 2019

materials, which is commonly used for large area and mass production of nanostructures. As a simple route to improve hardness, dielectric materials with relatively higher hardness, such as Al_2O_3, Cr_2O_3, ZrO_2, and TiO_2, etc., can be additionally coated on nanostructures, however, there is another critical issue on matching of refractive index between dielectrics and polymers, based on the effective medium theory [42–46]. To overcome material limitations and structural properties in nanophotonics, fine tailoring in nanostructures is required [47–49].

In our previous work, we designed and optimized each SWSs for several applications with different materials using optical simulation [50–55]. Based on these design schemes of SWSs, in this study, we present antireflective moth-eye structures (AMSs) with an oxide coating for hardness enhancement. AMSs are fabricated on PC substrate using hot embossing technique for large area production, and Al_2O_3, as a hardness enhancement layer, was coated by atomic layer deposition (ALD). Simulation results show RI profile and transmittance of AMSs for the filling fraction and thickness of Al_2O_3 coating layer. From these results, we propose the optimal design of Al_2O_3 coated AMSs. Experimentally, our fabricated sample shows hardness enhancement maintaining improved transmittance. In the process, we conducted the transmittance measurement and the scratch test in fabricated samples. Furthermore, we discuss optical properties for the morphology of AMSs with oxide coating layers.

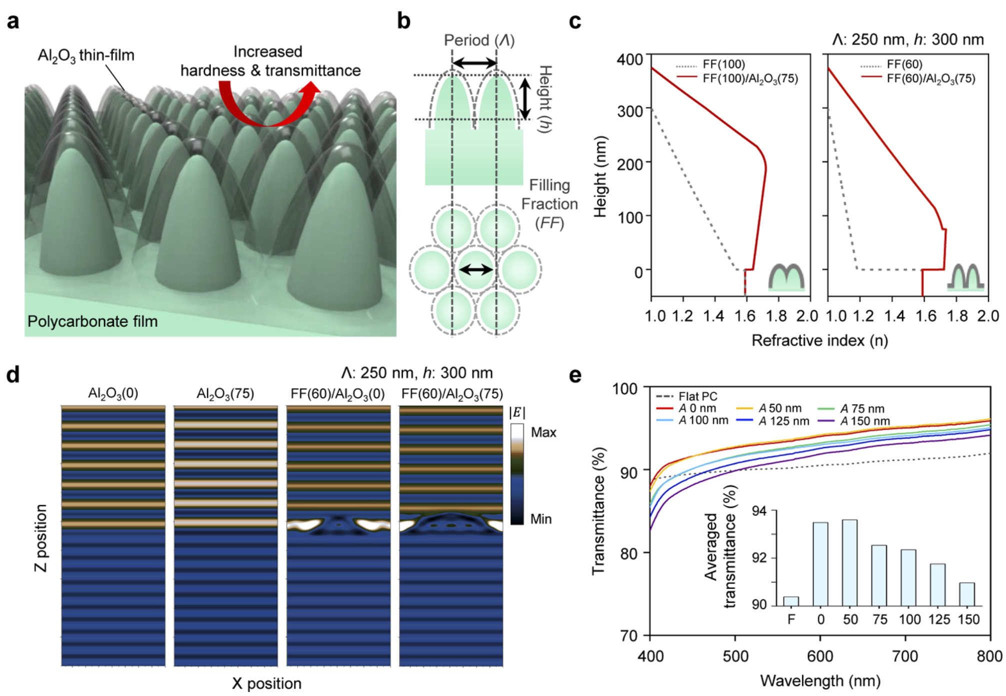

Fig. 1. Schematic illustration of antireflective moth-eye structures (AMSs) with Al_2O_3 monolayer on polycarbonate (PC) film. (b) Geometrical parameters of period, height, and filling fraction (FF) of AMSs (c) Calculated effective refractive indices of the Al_2O_3 coated AMSs on PC film. (d) Real part of electric-field distributions from three-dimensional finite-difference time-domain simulations. (e) Measured transmittances of fabricated samples with different Al_2O_3 coating thicknesses

2. Optical properties of Al_2O_3 coated PC films

Figure 1(a) shows the schematic illustration of antireflective moth-eye structures (AMSs) with Al_2O_3 monolayer coated on polycarbonate (PC) substrate for improvements of transmittance and surface hardness. The geometrical parameters such as period (Λ), height (h), and filling fraction (FF) were set to analyze optical performance depending on the parabolic moth-eye structure as shown in Fig. 1(b). The effective refractive indices were calculated with each FF factors of 60% and 100% with 75 nm Al_2O_3 thickness. In Fig. 1(c), the effective refractive indices were calculated by the volume weighted averaged refractive index between air and Al_2O_3 coated PC films depending on the nanostructure height [5, 56,57]. The abrupt change of effective refractive index was exhibited in FF 100% with 75 nm of Al_2O_3 layer, due to that Al_2O_3 has higher refractive index than PC film. By modifying structural parameter of FF, the effective refractive index was graded as shown in Fig. 1(c) right. In order to observe light propagations in antireflective films, the Al_2O_3 coated moth-eye structures were calculated at 500 nm wavelengths by rigorous coupled wave analysis (RCWA) with varying FF [58]. In E-field distribution, bare film, Al_2O_3 coating on bare film, moth-eye film, and Al_2O_3 coating on Moth-eye film were simulated for four cases. In the absence of the structure, high reflections were obtained due to the high refractive index of Al_2O_3. The results, on the other hand, show that the reflection of the AMSs with Al_2O_3 layer is significantly reduced. Transmittances of fabricated AMSs with different Al_2O_3 thicknesses were measured by spectrophotometer (Cary 500 Scan UV-Visible Spectrophotometer, Varian) from 400 nm to 800 nm wavelength ranges (Fig. 1e). The averaged transmittance (Fig. 1e inset) exhibited the increased transmittance of AMSs. Enhanced transmittances of AMSs on PC films were maintained with compared to the flat PC film even though of Al_2O_3 layer was coated.

3. Fabrication methods

Figure 2(a) shows the schemes of hot-embossing process using nanostructured nickel master stamp (HT-AR-02, Temicon) to achieve AMSs on PC substrate. The nickel mold was cleaned using acetone, isopropyl alcohol (IPA), and deionized (DI) water with blowing N_2 gas for self-assembled monolayer (SAM) treatment. The SAM of octadecyltrichlorosilane (OTS) was treated to nickel stamps for releasing a PC replica from the nickel stamp. The annealing process was subsequently performed for 5 min, at 120 °C using the hot plate. AMSs patterned PC samples were fabricated under the pressure of 20 bar, temperature of 120 °C at the glass transition temperature. Then, Al_2O_3 thin film was coated by using atomic layer deposition (Lucida D100 ALD system, NCD) at 80 °C. Trimethylaluminum (TMA) and H_2O were used as the precursor, and oxidant, respectively. The TMA pulse, N_2 purge, H_2O pulse, and N_2 purge cycle was repeated with base pressure of 500 mTorr and ~0.1 nm/cycle growth rate. The fabricated samples of photographs were shown in the Fig. 2(b), the glare-less PC films were obtained in all the antireflective films. The field emission scanning electron microscope (FE-SEM, S-4700, Hitachi) image was exhibited to figure out the uniformly coated Al_2O_3 on AMSs.

Optical Materials EXPRESS

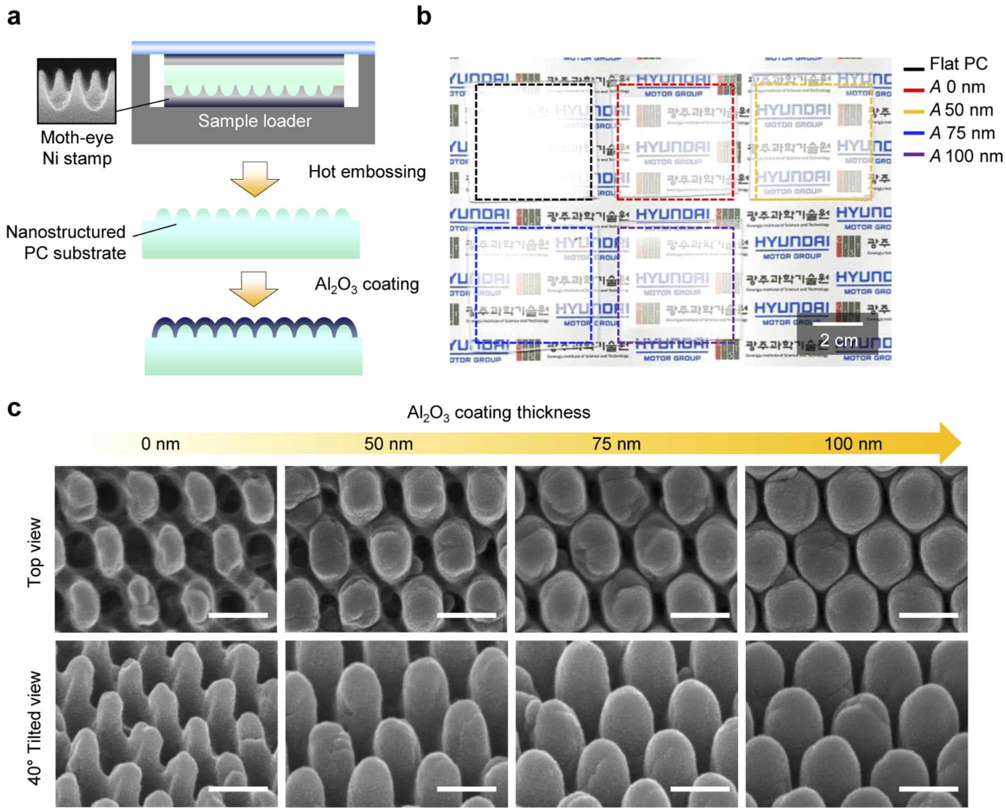

Fig. 2. (a) Fabrication steps for Al_2O_3 coated moth-eye polycarbonate films (b) Photographs of flat PC, moth-eye patterned PC, and Al_2O_3 coated moth-eye PC. (c) SEM images of top view and cross sectioned view for fabricated samples varying Al_2O_3 deposition thickness (0 nm, 50 nm, 75 nm, and 100 nm). The scale bar is 250 nm.

4. Nano-scratch testing of Al_2O_3 coated PC films

The mechanical property was measured by nano-scratch resistance measurement (NST^3, Anton Paar) with diamond stylus as illustrated in Fig. 3(a). The optical micrographs of fabricated samples with different Al_2O_3 thicknesses were shown in Fig. 3(b). The AMSs on PC film

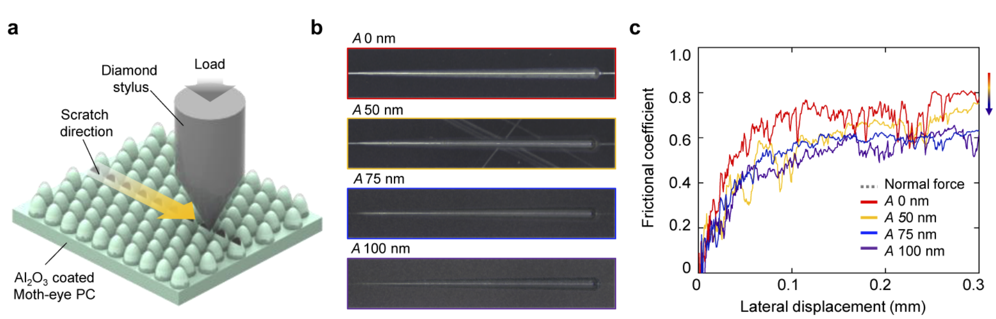

Fig. 3. (a) Schemes of scratch tests on samples (b) Optical microscope images of scratched Al_2O_3 coated moth-eye PC. (c) Frictional coefficient versus lateral displacement depending on the Al_2O_3 coating thickness.

without Al_2O_3 coating (*A* 0 nm) shows clear scratch marks. Also, as the thicknesses of Al_2O_3 are increased, gradually reduced scratch marks are observed. The scratch resistance was estimated by friction coefficient versus lateral displacement as shown in Fig. 3(c). The results show that the thicker Al_2O_3 increases the mechanical resistance. The average friction coefficient was reduced about 20% in *A* 100 nm samples compared to A 0 nm.

5. Optical simulations

To verify the optical properties of Al_2O_3/AMSs on PC films with varying geometric parameters for wide range applications, the numerical simulation was used. The rigorous coupled-wave analysis (RCWA) was exploited to obtain transmittance spectra for periodic AMSs on PC films (Diffract MOD, RSoft Design Group). In the RCWA calculation, a fifth diffraction order and periodic boundary conditions were set for the diffraction efficiency. The un-polarized light was achieved by averaging the TE/TM polarization. The normal incident plane wave was illuminated on Al_2O_3/PC nanostructures. Optical constants of PC and Al_2O_3 were measured by ellipsometer (UVISEL ER Benchtop AGAS, Horiba) and literature [57]. The material dispersion of optical constants was considered for wavelength dependent numerical simulations. Effective refractive indices were calculated by using MATLAB software (Mathworks, Inc) depending on their structural parameter (i.e., FF of AMSs and thickness of Al_2O_3) with the fixed factors (i.e., height of 300 nm and period of 250 nm), as shown in Fig. 4(a) and (b). Basically, the effective refractive index profile of AMSs is highly dependent on FF. The main reason is that the difference in effective refractive index between the AMSs and the PC substrate is determined by FF. Ideally, without Al_2O_3 coating, the closely packed AMSs (i.e., FF 100%) is the smoothest in the refractive index profile. However, since the Al_2O_3 coating causes an increase in the overall FF of the AMSs

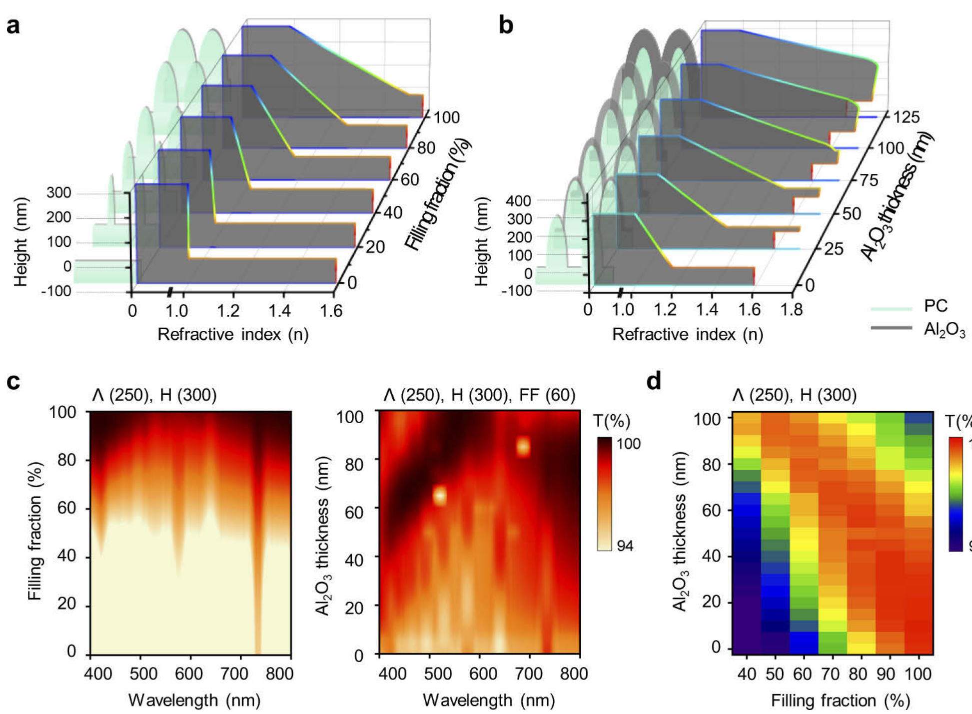

Fig. 4. Calculated refractive index depending on (a) FF and (b) Al_2O_3 thickness. (c) Contour plots of transmittance for FF and Al_2O_3 thickness. (d) Calculated average transmittance depending on Al_2O_3 thickness and FF.

Optical Materials EXPRESS

with Al_2O_3, the refractive index profile of the AMSs with Al_2O_3 were optimized at the Al_2O_3 thickness of 75 nm with FF 60% of AMSs. Figure 4(c) shows the contour plots of aforementioned geometries. In the case of AMSs without Al_2O_3 coating, the highest transmittance was obtained with FF 100%. The result shows a tendency for the transmittance to increase with FF of AMSs (Fig. 4(c) left). As shown in Fig. 4(c) right, the highest transmittance was observed in the 75 nm coated Al_2O_3. From these results, we note that the gradual profile of effective refractive index causes increased transmittance as suppressing surface reflection. Figure 4(d) shows the contour plot of the average transmittance of AMSs with Al_2O_3 thickness and FF. The result shows the correlation between Al_2O_3 thickness and FF in the transmittance of AMSs, which demonstrates the fact that AMSs with the lower FF require the thicker Al_2O_3 thickness for optimal transmittance.

To analyze geometrical effects, we considered the deformation of AMSs as a parabolic ratio defined by a geometrical change from the cylindrical shape (0%) to parabolic shape (100%), as shown in Fig. 5(a). With varying the parabolic ratio, we calculated the effective refractive index to form gradual profiles of effective refractive indices in Fig. 5(b). The refractive indices of AMSs without Al_2O_3 were varied by changing parabolic ratio (dot line). Relatively, the gradual profiles of effective refractive indices were achieved at the parabolic ratio from 60 to 100% (rigid line) with the fixed factors (i.e. Λ is 250 nm, h is 300 nm, and FF is 60%). Figure 5(c) shows the contour plots for transmittance of AMSs without and with Al_2O_3 coating (i.e., 75 nm). As a result, with Al_2O_3 coating, the improvement in transmittance was confirmed at 60 to 100%. Figure 5(d) shows the angle dependencies of Al_2O_3 coated moth-eye PC films, the improvement of transmittance was maintained until ~40 degree. Figure 5(e) shows the refractive indices of

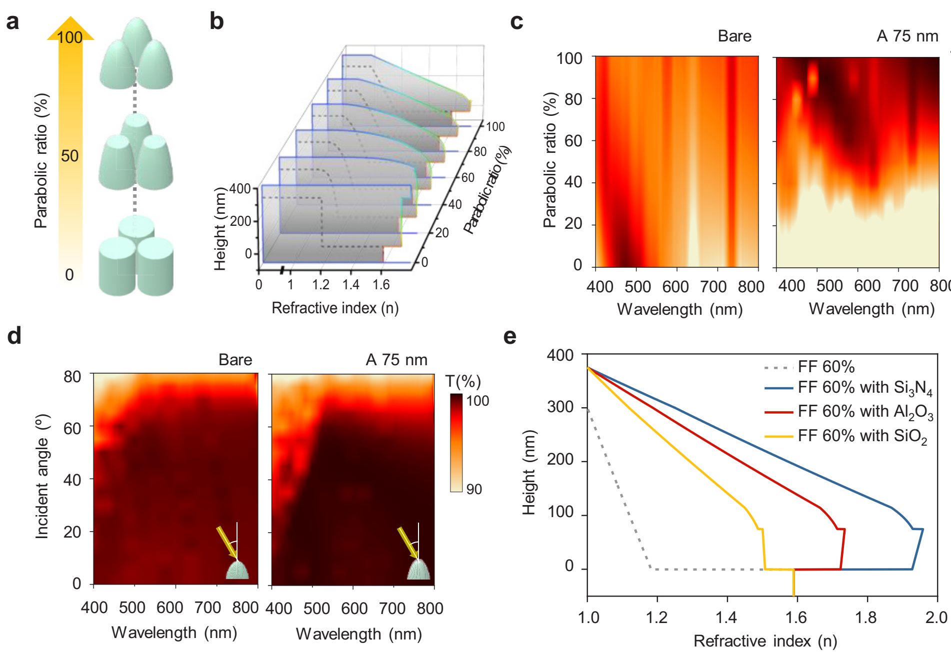

Fig. 5. (a) Schematic view of nanostructures with varying parabolic ratio. (b) Refractive index profile of AMSs for the parabolic ratio with Al_2O_3 coating (i.e., 75 nm). (c) Contour plots of transmittance of AMSs without and with Al_2O_3 coating (i.e., 75 nm). (d) Calculated transmittance depending on the angle of incident light. (e) Calculated refractive index with different coating materials (i.e., Si_3N_4 and SiO_2).

Optical Materials EXPRESS

different materials, and our proposed scheme can be varied by designs depending on the various applications with different materials.

6. Conclusion

We have designed and demonstrated the tailored Al_2O_3 coating on moth-eye structure for enhancing mechanical and optical performances. We confirmed that increased optical and mechanical properties were observed at uniformly coated Al_2O_3 monolayer by ALD deposition on the existed moth-eye antireflective structure. We calculate and modify the graded refractive index by varying structural parameter. The polycarbonate film coated with 75 nm Al_2O_3 thickness exhibits the smoothest graph at 75% of filling fraction than 100%, with the fixed factors (period is 250 nm and height is 300 nm). We notice that the effective refractive index easily calculated by volume weighted averaging method through nano-structure geometric design. Additionally, our proposed structure is applicable to various nanostructures which have different refractive index materials.

Funding

Hyundai Motor Group; National Research Foundation of Korea (2019H1A2A1060954, NRF2018M3D1A1039288); Korea Institute of Energy Technology Evaluation and Planning (20183010014310).

References

1. W. H. Southwell, "Gradient-index antireflection coatings," Opt. Lett. **8**(11), 584–586 (1983).
2. S. R. Kennedy and M. J. Brett, "Porous broadband antireflection coating by glancing angle deposition," Appl. Opt. **42**(22), 4573–4579 (2003).
3. S. A. Boden and D. M. Bagnall, "Tunable reflection minima of nanostructured antireflective surfaces," Appl. Phys. Lett. **93**(13), 133108 (2008).
4. M. Chen, H. C. Chang, A. S. Chang, S. Y. Lin, J. Q. Xi, and E. F. Schubert, "Design of optical path for wide-angle gradient-index antireflection coatings," Appl. Opt. **46**(26), 6533–6538 (2007).
5. H. K. Raut, V. A. Ganesh, A. S. Nair, and S. Ramakrishna, "Anti-reflective coatings: A critical, in-depth review," Energy Environ. Sci. **4**(10), 3779–3804 (2011).
6. W. K. Kuo, J. J. Hsu, C. K. Nien, and H. H. Yu, "Moth-eye-inspired biophotonic surfaces with antireflective and hydrophobic characteristics," ACS Appl. Mater. Interfaces **8**(46), 32021–32030 (2016).
7. G. Tan, J. H. Lee, Y. H. Lan, M. K. Wei, L. H. Peng, I. C. Cheng, and S. T. Wu, "Broadband antireflection film with moth-eye-like structure for flexible display applications," Optica **4**(7), 678–683 (2017).
8. K. X. Wang, Z. Yu, V. Liu, Y. Cui, and S. Fan, "Absorption enhancement in ultrathin crystalline silicon solar cells with antireflection and light-trapping nanocone gratings," Nano Lett. **12**(3), 1616–1619 (2012).
9. Y. J. Hung, S. L. Lee, and L. A. Coldren, "Deep and tapered silicon photonic crystals for achieving anti-reflection and enhanced absorption," Opt. Express **18**(7), 6841–6852 (2010).
10. H. S. Song, Y. J. Yoo, G. J. Lee, K. S. Chang, and Y. M Song, "Optical Design of Porous ZnO/TiO_2 Films for Highly Transparent Glasses with Broadband Ultraviolet Protection," J. Nanomater. **2017**, 1–8 (2017).
11. A. D. Ormonde, E. C. Hicks, J. Castillo, and R. P. Van Duyne, "Nanosphere Lithography: Fabrication of Large-Area Ag Nanoparticle Arrays by Convective Self-Assembly and Their Characterization by Scanning UV− Visible Extinction Spectroscopy," Langmuir **20**(16), 6927–6931 (2004).
12. Q. Chen, G. Hubbard, P. A. Shields, C. Liu, D. W. Allsopp, W. N. Wang, and S. Abbott, "Broadband moth-eye antireflection coatings fabricated by low-cost nanoimprinting," Appl. Phys. Lett. **94**(26), 263118 (2009).
13. Y. M. Song, S. J. Jang, J. S. Yu, and Y. T. Lee, "Bioinspired parabola subwavelength structures for improved broadband antireflection," Small **6**(9), 984–987 (2010).
14. Y. M. Song, E. S. Choi, G. C. Park, C. Y. Park, S. J. Jang, and Y. T. Lee, "Disordered antireflective nanostructures on GaN-based light-emitting diodes using Ag nanoparticles for improved light extraction efficiency," Appl. Phys. Lett. **97**(9), 093110 (2010).
15. K. Kurihara, Y. Saitou, N. Souma, S. Makihara, H. Kato, and T. Nakano, "Fabrication of nano-structure anti-reflective lens using platinum nanoparticles in injection moulding," Mater. Res. Express **2**(1), 015008 (2014).
16. T. Nakanishi, T. Hiraoka, A. Fujimoto, T. Okino, S. Sugimura, T. Shimada, and K. Asakawa, "Large area fabrication of moth-eye antireflection structures using self-assembled nanoparticles in combination with nanoimprinting," Jpn. J. Appl. Phys. **49**(7), 075001 (2010).

17. K. Choi, S. H. Park, Y. M. Song, C. Cho, and H. S. Lee, "Robustly nano-tailored honeycomb structure for high-throughput antireflection polymer films," J. Mater. Chem. **22**(33), 17037–17043 (2012).
18. M. Burghoorn, D. Roosen-Melsen, J. de Riet, S. Sabik, Z. Vroon, I. Yakimets, and P. Buskens, "Single layer broadband anti-reflective coatings for plastic substrates produced by full wafer and roll-to-roll step-and-flash nano-imprint lithography," Materials **6**(9), 3710–3726 (2013).
19. J. Zhang, S. Shen, X. X. Dong, and L. S. Chen, "Low-cost fabrication of large area sub-wavelength anti-reflective structures on polymer film using a soft PUA mold," Opt. Express **22**(2), 1842–1851 (2014).
20. C. Zhang, P. Yi, L. Peng, X. Lai, and J. Ni, "Fabrication of moth-eye nanostructure arrays using roll-to-roll UV-nanoimprint lithography with an anodic aluminum oxide mold," IEEE Trans. Nanotechnol. **14**(6), 1127–1137 (2015).
21. V. Garg, R. G. Mote, and J. Fu, "Rapid prototyping of highly ordered subwavelength silicon nanostructures with enhanced light trapping," Opt. Mater. **94**, 75–85 (2019).
22. C. J. Ting, M. C. Huang, H. Y. Tsai, C. P. Chou, and C. C. Fu, "Low cost fabrication of the large-area anti-reflection films from polymer by nanoimprint/hot-embossing technology," Nanotechnology **19**(20), 205301 (2008).
23. C. W. Kuo, J. Y. Shiu, Y. H. Cho, and P. E. I. L. I. N. Chen, "Fabrication of large-area periodic nanopillar arrays for nanoimprint lithography using polymer colloid masks," Adv. Mater. **15**(13), 1065–1068 (2003).
24. S. H. Ahn and L. J. Guo, "High-speed roll-to-roll nanoimprint lithography on flexible plastic substrates," Adv. Mater. **20**(11), 2044–2049 (2008).
25. S. H. Ahn and L. J. Guo, "Large-area roll-to-roll and roll-to-plate nanoimprint lithography: a step toward high-throughput application of continuous nanoimprinting," ACS Nano **3**(8), 2304–2310 (2009).
26. G. C. Park, Y. M. Song, J. H. Ha, and Y. T. Lee, "Broadband antireflective glasses with subwavelength structures using randomly distributed Ag nanoparticles," J. Nanosci. Nanotechnol. **11**(7), 6152–6156 (2011).
27. S. Ji, J. Park, and H. Lim, "Improved antireflection properties of moth eye mimicking nanopillars on transparent glass: flat antireflection and color tuning," Nanoscale **4**(15), 4603–4610 (2012).
28. J. W. Leem, Y. M. Song, and J. S. Yu, "Biomimetic artificial Si compound eye surface structures with broadband and wide-angle antireflection properties for Si-based optoelectronic applications," Nanoscale **5**(21), 10455–10460 (2013).
29. E. S. Choi, Y. M. Song, G. C. Park, and Y. T. Lee, "Disordered antireflective subwavelength structures using Ag nanoparticles for GaN-based optical device applications," J. Nanosci. Nanotechnol. **11**(2), 1342–1345 (2011).
30. J. J. Kim, Y. Lee, H. G. Kim, K. J. Choi, H. S. Kweon, S. Park, and K. H. Jeong, "Biologically inspired LED lens from cuticular nanostructures of firefly lantern," Proc. Natl. Acad. Sci. U. S. A. **109**(46), 18674–18678 (2012).
31. J. Tommila, V. Polojärvi, A. Aho, A. Tukiainen, J. Viheriälä, J. Salmi, A. Schramm, J. M. Konitio, A. Turtiainen, M. Niemi, and M. Guina, "Nanostructured broadband antireflection coatings on AlInP fabricated by nanoimprint lithography," Sol. Energy Mater. Sol. Cells **94**(10), 1845–1848 (2010).
32. Y. M. Song, Y. Jeong, C. I. Yeo, and Y. T. Lee, "Enhanced power generation in concentrated photovoltaics using broadband antireflective coverglasses with moth eye structures," Opt. Express **20**(S6), A916–A923 (2012).
33. A. Rahman, A. Ashraf, H. Xin, X. Tong, P. Sutter, M. D. Eisaman, and C. T. Black, "Sub-50-nm self-assembled nanotextures for enhanced broadband antireflection in silicon solar cells," Nat. Commun. **6**(1), 5963 (2015).
34. Y. Qiu, W. Liu, W. Chen, G. Zhou, P. C. Hsu, R. Zhang, Z. Liang, S. Fan, Y. Zhang, and Y. Cui, "Efficient solar-driven water splitting by nanocone $BiVO_4$-perovskite tandem cells," Sci. Adv. **2**(6), e1501764 (2016).
35. Y. J. Kim, G. J. Lee, S. Kim, J. W. Min, S. Y. Jeong, Y. J. Yoo, S. H. Lee, and Y. M. Song, "Efficient light absorption by GaN truncated nanocones for high performance water splitting applications," ACS Appl. Mater. Interfaces **10**(34), 28672–28678 (2018).
36. N. Yamada, T. Ijiro, E. Okamoto, K. Hayashi, and H. Masuda, "Characterization of antireflection moth-eye film on crystalline silicon photovoltaic module," Opt. Express **19**(S2), A118–A125 (2011).
37. S. Ji, K. Song, T. B. Nguyen, N. Kim, and H. Lim, "Optimal moth eye nanostructure array on transparent glass towards broadband antireflection," ACS Appl. Mater. Interfaces **5**(21), 10731–10737 (2013).
38. Y. J. Yoo, K. S. Chang, and Y. M. Song, "Design of ZnO hollow nanosphere arrays for UV absorbing transparent glasses," Opt. Quantum Electron. **48**(2), 88 (2016).
39. S. Jang, S. M. Kang, and M. Choi, "Multifunctional moth-eye TiO_2/PDMS pads with high transmittance and UV filtering," ACS Appl. Mater. Interfaces **9**(50), 44038–44044 (2017).
40. Q. D. Ou, Y. Q. Li, and J. X. Tang, "Light manipulation in organic photovoltaics," Adv. Sci. **3**(7), 1600123 (2016).
41. H. J. Jang, Y. J. Kim, Y. J. Yoo, G. J. Lee, M. S. Kim, K. S. Chang, and Y. M. Song, "Double-Sided Anti-Reflection Nanostructures on Optical Convex Lenses for Imaging Applications," Coatings **9**(6), 404 (2019).
42. J. Li, Y. Lu, P. Lan, X. Zhang, W. Xu, R. Tan, W. Song, and K. L. Choy, "Design, preparation, and durability of TiO_2/SiO_2 and ZrO_2/SiO_2 double-layer antireflective coatings in crystalline silicon solar modules," Sol. Energy **89**, 134–142 (2013).
43. C. C. Chang, T. Y. Oyang, F. H. Hwang, C. C. Chen, and L. P. Cheng, "Preparation of polymer/silica hybrid hard coatings with enhanced hydrophobicity on plastic substrates," J. Non-Cryst. Solids **358**(1), 72–76 (2012).
44. J. Lee, Y. Kim, H. Jang, and W. Chung, "Cr_2O_3 sealing of anodized aluminum alloy by heat treatment," Surf. Coat. Technol. **243**, 34–38 (2014).
45. S. Özel and E. Vural, "The microstructure and hardness properties of plasma sprayed Cr_2O_3/Al_2O_3 coatings," J. Optoelectron. Adv. M. **18**(11-12), 1052–1056 (2016).

Optical Materials EXPRESS

46. S. B. Khan, H. Wu, X. Huai, S. Zou, Y. Liu, and Z. Zhang, "Mechanically robust antireflective coatings," Nano Res. **11**(3), 1699–1713 (2018).
47. U. Cvelbar, K. K. Ostrikov, and M. Mozetic, "Reactive oxygen plasma-enabled synthesis of nanostructured CdO: tailoring nanostructures through plasma–surface interactions," Nanotechnology **19**(40), 405605 (2008).
48. J. Zhang, Y. Tang, K. Lee, and M. Ouyang, "Tailoring light–matter–spin interactions in colloidal hetero-nanostructures," Nature **466**(7302), 91–95 (2010).
49. P. Thébault, S. Niedermayer, S. Landis, N. Chaix, P. Guenoun, J. Daillant, and H. Orland, "Tailoring nanostructures using copolymer nanoimprint lithography," Adv. Mater. **24**(15), 1952–1955 (2012).
50. W. I. Nam, Y. J. Yoo, and Y. M. Song, "Geometrical shape design of nanophotonic surfaces for thin film solar cells," Opt. Express **24**(14), A1033–A1044 (2016).
51. K. Choi, S. H. Park, Y. M. Song, Y. T. Lee, C. K. Hwangbo, H. Yang, and H. S. Lee, "Nano-tailoring the surface structure for the monolithic high-performance antireflection polymer film," Adv. Mater. **22**(33), 3713–3718 (2010).
52. S. J. Jang, Y. M. Song, C. I. Yeo, C. Y. Park, J. S. Yu, and Y. T. Lee, "Antireflective property of thin film a-Si solar cell structures with graded refractive index structure," Opt. Express **19**(S2), A108–A117 (2011).
53. S. J. Jang, Y. M. Song, J. S. Yu, C. I. Yeo, and Y. T. Lee, "Antireflective properties of porous Si nanocolumnar structures with graded refractive index layers," Opt. Lett. **36**(2), 253–255 (2011).
54. G. C. Park, Y. M. Song, E. K. Kang, and Y. T. Lee, "Size-dependent optical behavior of disordered nanostructures on glass substrates," Appl. Opt. **51**(24), 5890–5896 (2012).
55. Y. J. Yoo, K. S. Chang, S. W. Hong, and Y. M. Song, "Design of ZnS antireflective microstructures for mid-and far-infrared applications," Opt. Quant. Electron. **47**(6), 1503–1508 (2015).
56. J. A. Dobrowolski, D. Poitras, P. Ma, H. Vakil, and M. Acree, "Toward perfect antireflection coatings: numerical investigation," Appl. Opt. **41**(16), 3075–3083 (2002).
57. M. M. Braun and L. Pilon, "Effective optical properties of non-absorbing nanoporous thin films," Thin Solid Films **496**(2), 505–514 (2006).
58. M. G. Moharam, "Coupled-wave analysis of two-dimensional dielectric gratings. In Holographic Optics: Design and Applications," Proc. SPIE **0883**, 8–12 (1988).
59. E. D. Palik, "Handbook of Optical Constants of Solids," 2nd ed. (Academic Press, 1985).